Lagrangian coherent structures separate dynamically distinct regions in fluid flows

Douglas H. Kelley, Michael R. Allshouse, and Nicholas T. Ouellette

Lagrangian Coherent Structures Separate Dynamically Distinct Regions in Fluid Flow

Douglas H. Kelley,[1] Michael R. Allshouse,[2] and Nicholas T. Ouellette[3, *]

[1]*Department of Materials Science & Engineering,*
Massachusetts Institute of Technology, Cambridge, Massachusetts 02139, USA
[2]*Department of Mechanical Engineering, Massachusetts Institute of Technology, Cambridge, Massachusetts 02139, USA*
[3]*Department of Mechanical Engineering & Materials Science,*
Yale University, New Haven, Connecticut 06520, USA

Using filter-space techniques, we study the scale-to-scale transport of energy in a quasi-two-dimensional, weakly turbulent fluid flow averaged along the trajectories of fluid elements. We find that although the spatial mean of this Lagrangian-averaged flux is nearly unchanged from its Eulerian counterpart, the spatial structure of the scale-to-scale energy flux changes significantly. In particular, its features appear to correlate with the positions of Lagrangian Coherent Structures (LCS). We show that the LCS tend to lie at zeros of the scale-to-scale flux, and therefore that the LCS separate regions that have qualitatively different dynamics. Since LCS are also known to be impenetrable barriers to advection and mixing, we therefore find that the fluid on either side of an LCS is both kinematically and dynamically distinct. Our results extend the utility of LCS by making clear the role they play in the flow dynamics in addition to the kinematics.

The complex nonequilibrium dynamics of flowing fluids are in principle completely described by the Navier–Stokes equations. For all but the simplest situations, however, these nonlinear partial differential equations are essentially intractable. Practical problems thus require either numerical solution of the equations, which brings its own difficulties, or some kind of suitable reduction of the complexity of the problem: one wishes to capture with as much fidelity as possible the full flow dynamics by considering only a finite number of degrees of freedom. Such an approach is ubiquitous in statistical physics; fluid mechanics, however, has so far resisted acceptable simplification by traditional techniques.

A possible reason for the failure of the usual tools of statistical mechanics to describe fluid flows is that we have not yet discovered the right degrees of freedom with which to describe the system. Although various ways to choose these degrees of freedom have been suggested [1, 2], perhaps none is more appealing than a decomposition of the flow into "coherent structures"—regions of the flow field that are distinguishable in time and space and over which some dynamical property or properties of the flow are strongly correlated. A huge variety of coherent structures have been described in fluid flows [3, 4]. Structures may be defined relative to a fixed coordinate system, in which case they are Eulerian, or relative to the motion of individual fluid elements, in which case they are Lagrangian. The canonical Eulerian structure is a vortex; the most common Lagrangian object is the so-called Lagrangian Coherent Structure (LCS) [5]. LCS are codimension-one material objects (*e.g.*, curves in a two-dimensional flow) that are the most important barriers to mixing of a passive scalar such as dye [6]. Much more difficult than defining structures, however, has been linking them quantitatively to flow dynamics. In partic-

ular, we seek connections between dynamical structures and the spectral transport of energy and momentum between different length and time scales that makes Navier–Stokes dynamics both rich and difficult to describe.

In this Letter, we demonstrate such a link for a particular type of coherent structure in an experimental quasi-two-dimensional, weakly turbulent flow. To determine the spectral dynamics of the flow, we use filter-space techniques [7–13] to measure the scale-to-scale flux of energy as a function of space and time. As we showed previously, this energy flux is persistent along the Lagrangian trajectories of fluid elements [14]. We therefore developed a novel analysis tool, averaging the flux along such trajectories to produce Lagrangian-averaged flux fields. These new fields have features that align strikingly well with LCS; indeed, the LCS frequently lie along zeros of the Lagrangian-averaged flux. By measuring the change in flux along line segments that are locally transverse to LCS, we find this observation to be statistically robust: on the average, LCS separate regions of scale-to-scale energy flux of opposite sign. Thus, we show that LCS, whose role as kinematic transport barriers is well established [15], also play a key role in the flow *dynamics*. Our observations bolster the growing consensus that LCS are a very promising type of coherent structure for tractably describing complex fluid flows, and demonstrate a clear connection between a particular type of coherent structure and the nonlinear dynamics of the flow.

Our experimental data come from a quasi-two-dimensional electromagnetically driven thin-layer flow that is described in detail elsewhere [16, 17]. A layer of salt water (4 mm × 86 cm × 86 cm, 16% NaCl by mass) lies below a similarly thin layer of fresh water and above a square array of permanent magnets arranged in stripes of alternating polarity. The half-wavelength of the

stripe pattern is $L = 2.54$ cm; each magnet is 1.27 cm in diameter and has a magnetic field of roughly 0.3 T at its surface [18]. Imposing a steady electric current through the salt water produces Lorentz forces that drive fluid motion, which becomes unsteady, spatially disordered, and weakly turbulent when the current is large. In the results discussed below, the Reynolds number is $Re = UL/\nu = 220$ (where U is the measured root-mean-square velocity and ν is the kinematic viscosity), well into the disordered regime. The Reynolds number defined in this way characterizes the nondimensional strength of the forcing rather than the extent of any turbulent cascades. We seed the flow with 51 μm fluorescent tracer particles that lie on the interface between the salt water layer and the less-dense fresh water layer, and the particles accurately track the fluid motion [19]. We image them with a 4 megapixel digital camera at 60 frames per second, avoiding possible boundary effects by limiting the field of view to a central 32 cm × 24 cm region. In the resulting movies we track about 35 000 particles per frame with a multi-frame predictive tracking algorithm [20]. Although the particle loading is high, they are typically separated by at least 15 diameters and so are unlikely to interact. We measure Lagrangian particle velocities by differentiating the trajectories. Eulerian velocity fields are then produced by projecting the spatially dense Lagrangian data onto a basis of incompressible streamfunction eigenmodes [16]. Because particles are confined to the interface and because the basis is carefully chosen, the resulting velocity fields approximate two-dimensional, incompressible flow very closely.

We locate the LCS in the velocity fields using the recently described method based on geodesics of the Riemannian metric derived from the Cauchy–Green strain tensor [21]. We use a modified algorithm to locate the hyperbolic transport barriers (LCS) from the experimental data [22]. The algorithm takes in the experimentally measured velocity field and smooths the data in space to remove noise in the velocity gradient fields. For the defined time interval, a flow map is calculated and the corresponding Cauchy–Green tensor is calculated at each point. The eigenvalues and eigenvectors of the Cauchy–Green tensor correspond respectively to the local stretching rates and directions of fluid elements. The eigenvector corresponding to the smaller eigenvalue forms a vector field that is everywhere tangent to the LCS. Using this property, we calculate strainlines (trajectories of the eigenvector field) and apply the necessary conditions to identify the LCS [21].

To obtain scale-to-scale energy flux fields, we use a filter-space technique (FST) [8–10]. The idea of an FST is straightforward. Briefly, applying a low-pass spatial filter to the equation of motion for energy yields a new expression. Each term in the filtered equation corresponds to a term in the original equation, with one exception: a new term that arises from the nonlinearity that accounts
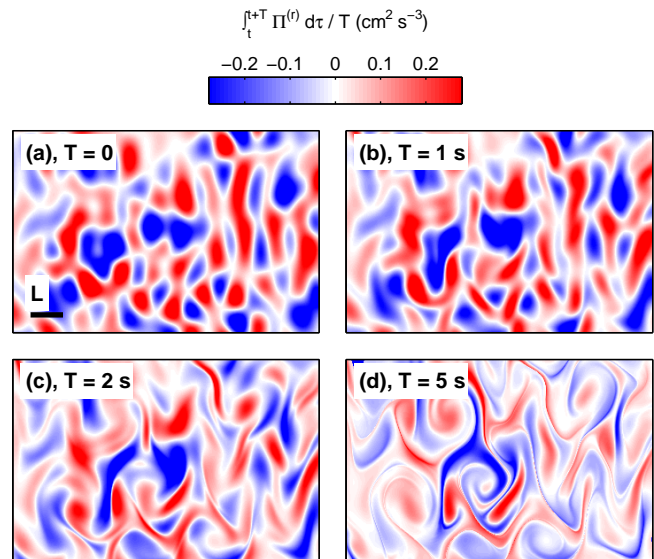

FIG. 1. (color online.) Example scale-to-scale energy flux fields. (a) Flux field with no Lagrangian averaging ($T = 0$). (b–d) Lagrangian-averaged flux fields, with averaging time $T = 1$ s, $T = 2$ s, and $T = 5$ s, respectively. The scale bar indicates the forcing length L, and the filter scale is $r/L = 1.75$ in all cases.

for coupling between the scales removed by the filter and the scales that are retained. This term, analogous to the Reynolds stress that appears when the Navier–Stokes equations are averaged, directly measures the energy flux $\Pi^{(r)}$ through the filter scale r. But unlike assessing the spectral properties of the flow by working in the Fourier domain, $\Pi^{(r)}$ is a function of space, and is given by

$$\Pi^{(r)} = -\left[(u_i u_j)^{(r)} - u_i^{(r)} u_j^{(r)} \right] \partial_i u_j^{(r)}. \qquad (1)$$

Here u_i is a velocity component; summation is implied over repeated subscripts. The superscript (r) denotes filtered quantities with length scales smaller than r removed. Following previous work [10, 14], we used a low-pass Gaussian filter to implement the FST because it is well behaved in both real space and frequency space. With this sign convention, $\Pi^{(r)} > 0$ denotes transfer to smaller scales (larger wavenumbers), and $\Pi^{(r)} < 0$ denotes transfer to larger scales (smaller wavenumbers). An example scale-to-scale energy flux field, with $r/L = 1.75$ where the spatially averaged flux vanishes, is shown in Fig. 1a. The spatial resolution is about 1.5 mm, the typical distance between tracked particles.

$\Pi^{(r)}$ is itself a dynamical variable, and the energy flux fields are not stationary in time. Thus, it is natural to ask what energy flux a fluid element experiences as it is swept along by the flow [14]. In particular, we consider the average scale-to-scale energy flux along Lagrangian trajectories. Rather than using measured trajectories, which can be short, to make this calculation, we construct

Lagrangian trajectories by *a posteriori* integrating the equations of motion of virtual tracers through the time-resolved velocity fields [6, 23]. The virtual tracers sample the time-resolved energy-flux fields as they move. We define the Lagrangian-averaged energy flux over a time T as

$$\frac{1}{T} \int_t^{t+T} \Pi^{(r)}(\mathbf{x}(\tau)) \, \mathrm{d}\tau, \tag{2}$$

where the integral is taken over a Lagrangian trajectory $x(\tau)$. By uniformly seeding the entire observation region with virtual tracers, we can measure the Lagrangian-averaged flux as a function of space, as shown in fig. 1b–d. In principle it would be possible to measure Lagrangian-averaged flux along observed trajectories of actual particles as well, but it is typically much noisier due to short or broken trajectories [6, 23]. As the averaging time T increases, the scale-to-scale energy flux field is stretched and folded in a manner reminiscent of scalar mixing.

To examine the convergence properties of this Lagrangian-averaged flux, we compared its spatial average as a function of T with the corresponding spatial average of the instantaneous, Eulerian flux field. In two-dimensional turbulence, energy is expected to be transported from the scale at which it is injected to larger length scales (smaller wavenumbers) in an inverse energy cascade [24]. In terms of $\Pi^{(r)}$, we would expect negative values on the average for length scales $r \gtrsim L$. In fig. 2, we show the spatially averaged scale-to-scale energy flux as a function of r for Lagrangian averaging times ranging from $T = 0$ (the Eulerian case) to 10 s. Note that the eddy turnover time of our flow, defined simply as the ratio of L to the root-mean-square velocity, is 2.4 s. Although the Lagrangian-averaged flux is not identical to the Eulerian case, the overall shape and behavior are very similar. As expected, $\langle \Pi^{(r)} \rangle > 0$ for small r and $\langle \Pi^{(r)} \rangle < 0$ for large r, with $\langle \Pi^{(r)} \rangle = 0$ at $r/L = 1.75$. Thus, the Lagrangian averaging appears to be well behaved.

Having shown that these Lagrangian-averaged flux fields are statistically reasonable, we now consider more carefully their spatial structure. As we mentioned above, the features of these fields resemble the stretched and folded patterns commonly observed when a passive scalar such as dye is mixed by fluid advection. In the passive scalar case, the mixing is known to be organized by LCS [6]. Surprisingly, we find the same phenomenon for our Lagrangian-averaged scale-to-scale energy flux fields: the LCS appear to organize this dynamical field, which is certainly not passive, as well.

Figure 3a shows the same Lagrangian-averaged flux field as in fig. 1d, but now with the LCS overlaid. We calculated the LCS over a 5 s time window (approximately two eddy turnover times), matching the time T used for the Lagrangian averaging. The correspondence between the LCS and the Lagrangian-averaged flux is immediately apparent; in particular, the LCS lie nearly
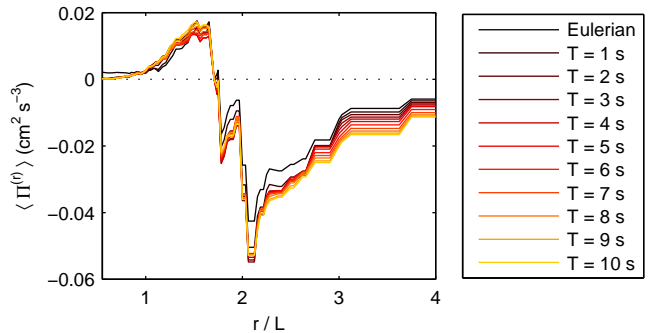

FIG. 2. (color online.) Spatial mean of the Lagrangian-averaged flux as a function of filter scale, for different averaging times T. Although the details change somewhat from the Eulerian case ($T = 0$) to the Lagrangian case, the qualitative behavior is very similar.

at the zeros of the flux field, and thus tend to separate regions with oppositely signed Lagrangian-averaged flux. To show this result in more detail, a portion of the flux field is magnified in fig. 3b. We note that the LCS do not match the zeros of the flux field exactly; nonetheless, the correspondence is remarkably close. To quantify it, we measured the variation of the Lagrangian-averaged flux over short line segments transverse to the LCS, as shown in gray in fig. 3b. In fig. 3c, we show the variation of the Lagrangian-averaged flux along this example transverse line segment. Consistent with our qualitative observations, the Lagrangian-averaged flux is negative on one side of the LCS, positive on the other, and passes through zero near the point where the transverse line segment intersects the LCS.

To quantify the relationship between LCS and the Lagrangian-averaged energy flux statistically, we decorated all the LCS with such transverse line segments all along their lengths, found the flux along each segment, and computed the overall average of the ensemble of 6.5×10^5 segments. The result, also plotted in fig. 3c, confirms our observations from the example segment: the Lagrangian-averaged energy flux is zero near LCS, positive on one side, and negative on the other. On average, the distance between an LCS and the zero-flux contour is 0.067 cm; to experimental precision, they coincide. Note that we assign a directionality to each line segment so that the energy flux increases from left to right; otherwise, the average over the ensemble would vanish since the Lagrangian-averaged flux is equally likely to be positive or negative on any given side of an LCS. The magnitude of the flux, however, is unchanged by our choice of directionality. And indeed, this magnitude is on the order of 0.05 cm^{2}s^{-3}, much larger than the overall spatial average of 0.01 cm^{2}s^{-3}. Thus, our results are statistically significant, and indicate that LCS do tend to separate regions of oppositely signed Lagrangian-averaged energy

$\int_t^{t+T} \Pi^{(r)} \, d\tau \, / \, T \; (\mathrm{cm}^2 \, \mathrm{s}^{-3})$

−0.2 −0.1 0 0.1 0.2

(a)

L

(b)

(c) — example — ensemble mean

flux along transverses (cm^2 s^{-3})

0.3
0.2
0.1
0
−0.1
−0.2

−0.6 −0.4 −0.2 0 0.2 0.4 0.6
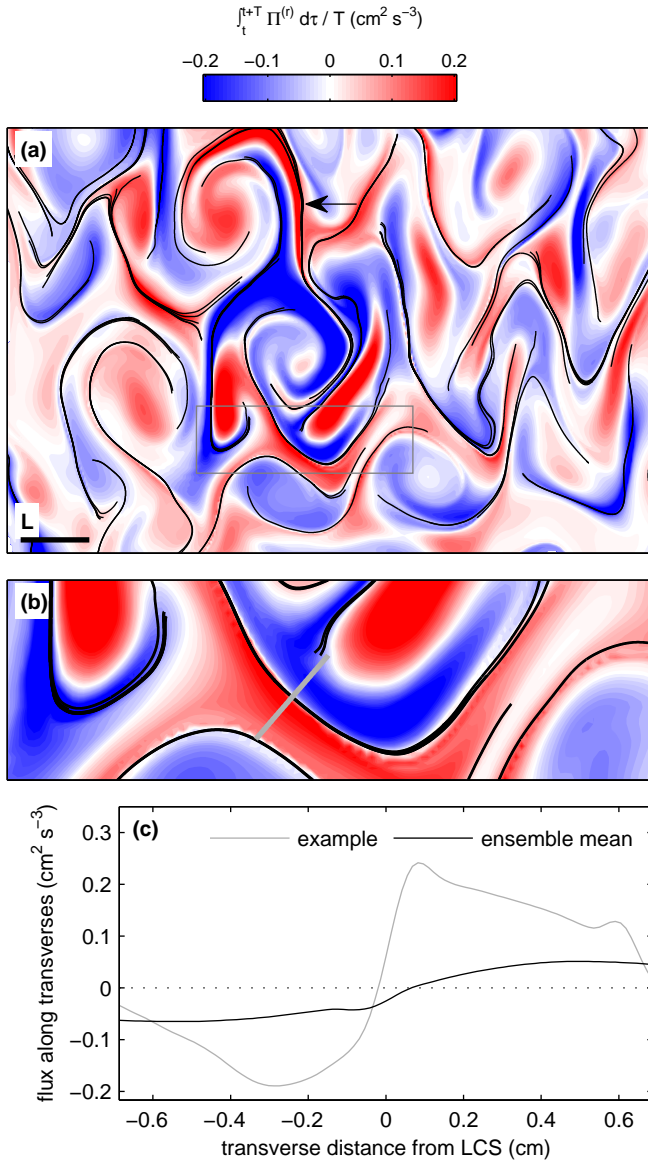
transverse distance from LCS (cm)

FIG. 3. (color online.) Lagrangian-averaged scale-to-scale energy flux and LCS. (a) The same Lagrangian-averaged flux field shown in Fig. 1d with the LCS overlaid. The scale bar indicates the forcing length L. LCS tend to separate regions of opposite energy flux. (b) A magnified view of the same flux field and LCS shown in (a). An example line segment perpendicular to an LCS is shown in gray. (c) The Lagrangian-averaged flux along the example transverse line shown in (b), plotted in gray, and the flux averaged over the full ensemble of transverse lines. On the average, LCS separate regions of scale-to-scale energy flux of opposite sign.

flux, and therefore regions that are dynamically distinct.

Although this lowest-order statistical characterization is clear, deviations do occur. Not every LCS separates regions of oppositely signed flux, nor does every LCS lie on zeros of the Lagrangian-averaged flux. In Figure 3, however, we have only shown the Lagrangian-averaged flux
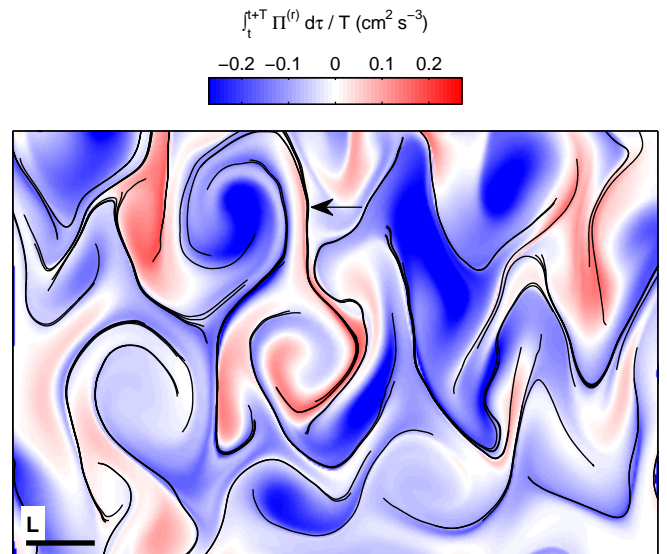
$\int_t^{t+T} \Pi^{(r)} \, d\tau \, / \, T \; (\mathrm{cm}^2 \, \mathrm{s}^{-3})$

−0.2 −0.1 0 0.1 0.2

L

FIG. 4. LCS and Lagrangian-averaged energy flux through scale $r/L = 2.09$. The scale bar indicates the forcing length L. At different scales, different LCS align with zeros of scale-to-scale energy flux.

fields for a filter scale of $r/L = 1.75$. Figure 4 overlays LCS on the Lagrangian-averaged flux through a different length scale, $r/L = 2.09$, where the inverse energy transfer is the strongest. Comparing, we observe LCS that lie on zeros of the flux field at one scale, but not another (one is marked with an arrow). This result suggests that each LCS has a characteristic dynamical length scale at which it best divides the Lagrangian-averaged energy flux. We also note that although we expect our results to remain valid at higher Reynolds numbers, we cannot access them in our current apparatus without driving substantial out-of-plane flow [16]. Future studies will explore these questions and hypotheses.

To summarize, by defining a Lagrangian-averaged scale-to-scale energy flux and comparing its spatial structure to LCS, we have shown that LCS, on average, separate regions of opposite energy flux in quasi-two-dimensional weak turbulence. Our findings add a link between LCS and the flow dynamics to the already well established connection between LCS and flow kinematics, thus enhancing our understanding of the role played by LCS and solidifying the choice of LCS as a "good" set of coherent structures for decomposing complex flow fields. Future work, and particularly future theoretical studies, should aim to place our empirical findings on a stronger mathematical foundation.

* nicholas.ouellette@yale.edu

[1] D. A. Egolf, Science **287**, 101 (2000).
[2] M. P. Fishman and D. A. Egolf, Phys. Rev. Lett. **96**, 054103 (2006).
[3] A. K. M. F. Hussain, J. Fluid Mech. **173**, 303 (1986).
[4] N. T. Ouellette, C. R. Physique **13**, 866 (2012).
[5] G. Haller and G. Yuan, Physica D **147**, 352 (2000).
[6] G. A. Voth, G. Haller, and J. P. Gollub, Phys. Rev. Lett. **88**, 254501 (2002).
[7] M. Germano, J. Fluid Mech. **238**, 325 (1992).
[8] S. Liu, C. Meneveau, and J. Katz, J. Fluid Mech. **275**, 83 (1994).
[9] G. L. Eyink, J. Stat. Phys. **78**, 335 (1995).
[10] M. K. Rivera, W. B. Daniel, S. Y. Chen, and R. E. Ecke, Phys. Rev. Lett. **90**, 104502 (2003).
[11] S. Chen, R. E. Ecke, G. L. Eyink, X. Wang, and Z. Xiao, Phys. Rev. Lett. **91**, 214501 (2003).
[12] S. Chen, R. E. Ecke, G. L. Eyink, M. Rivera, M. Wan, and Z. Xiao, Phys. Rev. Lett. **96**, 084502 (2006).
[13] M. Wan, Z. Xiao, C. Meneveau, G. L. Eyink, and S. Chen, Phys. Fluids **22**, 061702 (2010).
[14] D. H. Kelley and N. T. Ouellette, Phys. Fluids **23**, 115101 (2011).
[15] S. C. Shadden, F. Lekien, and J. E. Marsden, Physica D **212**, 271 (2005).
[16] D. H. Kelley and N. T. Ouellette, Phys. Fluids **23**, 045103 (2011).
[17] Y. Liao, D. H. Kelley, and N. T. Ouellette, Phys. Rev. E **86**, 036306 (2012).
[18] D. H. Kelley and N. T. Ouellette, Am. J. Phys. **79**, 267 (2011).
[19] N. T. Ouellette, P. J. J. O'Malley, and J. P. Gollub, Phys. Rev. Lett. **101**, 174504 (2008).
[20] N. T. Ouellette, H. Xu, and E. Bodenschatz, Exp. Fluids **40**, 301 (2006).
[21] G. Haller and F. J. Beron-Vera, Physica D **241**, 1680 (2012).
[22] M. R. Allshouse, J.-L. Thiffeault, and T. Peacock, to appear (2013).
[23] S. T. Merrifield, D. H. Kelley, and N. T. Ouellette, Phys. Rev. Lett. **104**, 254501 (2010).
[24] R. H. Kraichnan, Phys. Fluids **10**, 1417 (1967).